



# Simulating compound flooding events in a hurricane

Yinglong J. Zhang<sup>1</sup> · Fei Ye<sup>1</sup> · Haocheng Yu<sup>1</sup> · Weiling Sun<sup>1</sup> · Saeed Moghimi<sup>2</sup> · Edward Myers<sup>2</sup> · Karinna Nunez<sup>1</sup> · Ruoyin Zhang<sup>3</sup> · Harry Wang<sup>1</sup> · Aron Roland<sup>4</sup> · Jiabi Du<sup>5</sup> · Zhuo Liu<sup>6</sup>

Received: 26 August 2019 / Accepted: 29 January 2020 / Published online: 27 February 2020  
© Springer-Verlag GmbH Germany, part of Springer Nature 2020

## Abstract

Compound flooding is usually induced by the concurrence of coastal storm surge and heavy precipitation induced river flooding, with the former involving oceanic processes and the latter involving hydrological processes. The simulation of these two types of processes is traditionally handled by two different types of models separately, i.e., hydrological models (e.g., NOAA's National Water Model (NWM)) and hydrodynamic models. This dichotomy leaves gaps in simulating the interrelated processes in a holistic fashion. In this paper, we present a creek-to-ocean 3D baroclinic model based on SCHISM (Semi-implicit Cross-scale Hydroscience Integrated System Model) that aims to unite traditional hydrologic and hydrodynamic models in a single modeling platform to simulate compound floods, by taking full advantage of the model polymorphism (i.e., a single model grid can seamlessly morph between full 3D, 2DV, 2DH, and quasi-1D modes). Using Hurricane Irene's impact on Delaware Bay as an example, a seamless 2D-3D model grid is implemented to include the entire US East Coast and Gulf of Mexico with a highly resolved Delaware Bay (down to 20-m resolution). The streamflow from NWM is injected into SCHISM grid at the intersections of NWM's segments and SCHISM's land boundary, and the pluvial and fluvial processes are directly handled by SCHISM. We demonstrate the model's accuracy, stability, and robustness with focus on the compound flooding events. The relative role of different physical processes in such events is examined by a series of sensitivity tests. Our results confirm the occurrence of backwater process into far upstream rivers and creeks and thus demonstrate the need for a dynamic two-way coupling between the hydrodynamic and hydrological models.

**Keywords** Compound flooding · Backwater effect · National Water Model · SCHISM · Delaware Bay · USA

## 1 Introduction

---

Responsible Editor: Amin Chabchoub

---

Yinglong J. Zhang  
yjzhang@vims.edu

<sup>1</sup> Virginia Institute of Marine Science, College of William & Mary, Gloucester Point, VA 23062, USA

<sup>2</sup> Coast Survey Development Laboratory, NOAA, Silver Spring, MD 20910, USA

<sup>3</sup> State Key Laboratory of Hydroscience and Engineering, Tsinghua University, Beijing 100084, China

<sup>4</sup> BGS IT&E GmbH, Darmstadt, Germany

<sup>5</sup> Applied Ocean Physics and Engineering Department, Woods Hole Oceanographic Institution, Woods Hole, MA 02543, USA

<sup>6</sup> One Concern, Inc., Menlo Park, CA 94025, USA

Compound flooding, usually caused by the concurrence of coastal storm surge and heavy precipitation and river flooding, is inherently challenging to study as it involves multiple processes that occur at drastically different temporal and spatial scales (storm surge, pluvial and fluvial inundation, and groundwater processes). The simulation of these processes is traditionally handled by two different types of models separately, i.e., hydrologic models (e.g., National Water Model (NWM)) and hydrodynamic models, and so far, only a subset of these processes have been studied using a single model or coupled modeling system (Kerr et al. 2013; Chen et al. 2013; Cho et al. 2012; Dresback et al. 2013; Teng et al. 2017; Wing et al. 2019). The dichotomy leaves gaps in simulating the interrelated processes (e.g., backwater effect) in a holistic fashion. For example, in the coastal zone, the hydrological models cannot handle some surface flow processes that are

connected to the estuarine processes. On the other hand, simulating compound flooding in hydrometeorological events with a hydrodynamic model is inherently challenging because it involves pluvial and fluvial processes that are typically handled by hydrological and hydraulic models (Bilskie and Hagen 2018; Moftakhari et al. 2019). Particularly lacking is a tight-coupling procedure that can accurately represent the complex physical interactions between storm surge and rainfall-runoff (Santiago-Collazo et al. 2019). On the other hand, “implementation of full- and tight-coupling for these types of numerical models (e.g. hydrologic, ocean circulation, and hydraulic model) is more complicated than loose- or one-way coupling, and this difficulty is attributed to the complex mathematical representation of their physical processes, the computational power required, and the temporal and spatial resolution (varying time and length scales) of the numerical models” (Santiago-Collazo et al. 2019). The current paper presents a first attempt to develop a tightly coupled hydrologic-hydrodynamic model and its application to a compound flooding study.

The need for accurately predicting the compound flooding events has become more urgent because of recent occurrences of “wet storms” (with accompanying heavy precipitation) such as Hurricanes Harvey (2018) and Florence (2018), and prediction of more frequent wet storms in the future by many climate models (Groisman et al. 2001, 2004; Dettinger 2011; Sobel et al. 2016; Trenberth et al. 2018; Trenberth 2011). The occurrence of compound flooding events in some of these wet storms demands advanced simulation tools for risk assessment and forecast. To this end, National Oceanic and Atmospheric Administration (NOAA) has initiated the NOAA Water Initiative to understand, develop, demonstrate, and implement an improved total water level prediction that includes propagating up- and downstream signals in coastal and estuarine as well as in the riverine system, particularly during storm events. The goal is to establish an integrated water forecasting system that covers inland and coastal waters to provide vital information to end users and stakeholders. This paper documents our contributions to the Water Initiative project, using a seamless creek-to-ocean 3D baroclinic unstructured-grid (UG) model (SCHISM, schism.wiki, last accessed in July 2019; Zhang et al. 2016), forced by the predicted flows from a continental scale hydrological model (NWM; <https://water.noaa.gov/about/nwm>, last accessed in July 2019) at the 10-m contour above mean sea level (MSL), with application to Hurricane Irene (2011) near the Delaware Bay to holistically simulate the total water level and its individual components.

Our focus in this paper is the hydrological regime and its interaction with the coastal regime in the form of compound flooding; a companion paper (Ye et al. 2020) deals with the

interaction between the oceanic and estuarine regimes. The goal here is to directly simulate some hydrological/hydraulic processes<sup>1</sup> in a hydrodynamic model so as to simplify the coupling procedure with the NWM. In doing so, we are able to use a single model to simulate processes from deep ocean to beyond the “head of tide.” Two key technological enablers for this new capability are (1) the semi-implicit framework employed in SCHISM that greatly enhances numerical stability and robustness; (2) model polymorphism (i.e., a single model grid can seamlessly morph between full 3D, 2DV, 2DH, and quasi-1D modes) that results in great efficiency. We remark that the model has been extensively benchmarked previously with a number of hydraulic test cases in the context of tsunami inundation (NTHMP 2012; Lynett et al. 2017). The model has also been successfully applied to some creek-to-ocean systems (Yu et al. 2017) and systems beyond the head of tide (Ateljevich 2014). In addition, the modeling system has incorporated a variety of hydraulic modules for weirs, culverts, gates, etc. (Ateljevich 2014) that can be invoked if proved necessary in the future.

To demonstrate the model’s capability to simulate some small-scale processes in the hydrological and hydraulic regime, we first present in Section 2 two benchmark tests for precipitation driven inundation and hydraulic jump behind a weir. Then, in Section 3, we validate the model for Hurricane Irene (2011) near Delaware Bay, with focus on river stages and flows at some upstream river gauges. Through a series of sensitivity tests, we analyze in Section 4 the interactions between coastal and riverine regimes. Specifically, we study the sensitivity to the grid resolution in the hydrological regime, the river influence on the Bay, the effects of directly incorporating precipitation in the study domain, and backwater effect from coastal ocean into upstream rivers and creeks. As far as the model coupling between SCHISM and NWM (at SCHISM’s boundary) is concerned, two important questions are (1) whether two-way feedback is significant and (2) where to place the boundary between the two models. We demonstrate that despite that fact that we have placed the boundary at 10 m above sea level, the backwater effect can still propagate far upstream and reach the boundary of our study domain. Therefore, the current approach of one-way coupling between NWM and SCHISM needs to be revised in the future to

<sup>1</sup> Note that hydrological models are designed to handle not only surface water processes but also other aspects of a hydrological cycle such as groundwater flow and evapotranspiration. However, if we focus on the surface water processes alone as a first step, a hydrodynamic model can in theory be used to study the compound flooding events. This is a good starting point for the nearshore areas because the groundwater effects are often considered secondary there and, in many cases, can be accounted for by using some simplified approaches such as volume sources and sinks. However, a fully coupled surface-groundwater model may be necessary in some coastal zones to accurately account for the water budget. As a first step, the use of a unified modeling framework in the form of a hydrodynamic model for the coastal zone is obviously advantageous as it greatly simplifies the model coupling procedure down the road.

eventually include the two-way feedback. A brief summary of the main findings is presented in Section 5.

## 2 Benchmark tests for some hydrological and hydraulic processes

### 2.1 Numerical model

SCHISM is a seamless cross-scale hydrodynamic model grounded on unstructured hybrid triangular-quadrangular grids in the horizontal and hybrid localized sigma coordinates in the vertical (Zhang et al. 2015, 2016). Like its predecessor SELFE (Zhang and Baptista 2008a), it employs a highly efficient semi-implicit scheme to bypass terms that place most stringent stability constraints and thus achieves great efficiency even under very fine resolution down to a few meters (Liu et al. 2018). The model polymorphism is achieved with the use of flexible 3D gridding system and a single SCHISM grid can morph between 3D, 2DH, 2DV, and quasi-1D configurations in different parts of the domain, resulting in great efficiency for cross-scale applications. The use of shaved cells near the bottom faithfully preserves the original bathymetry and greatly improves the simulation of near-bottom processes (salt intrusion, gravity overflow, etc.). No bathymetry smoothing is necessary with SCHISM and the detrimental effects of the smoothing on estuarine physics have been described in Ye et al. (2018). The very robust wetting and drying scheme used in SCHISM (Zhang and Baptista 2008b; Zhang et al. 2011) is instrumental in pushing this model into the hydrological regime.

### 2.2 Reservoir test

Simulating precipitation-induced inundation is very challenging for hydrodynamic models that are usually based on shallow-water equations. A very thin layer of water is initially formed on the dry ground with a primary force balance formed between gravity and bottom friction. The flow is friction dominated initially and has a low Reynolds number, and the friction coefficient is usually an order of magnitude larger than the commonly used values in coastal settings (McKeon et al. 2004). The combination of the large friction, steep slopes (which are common in hydrological regime), and strong and dynamic wetting and drying presents formidable challenges to hydrodynamic models. An alternative to circumvent this challenge (and to reduce computational cost) is to use reduced form of the shallow water equations as commonly adopted in hydrological models. In the coastal zone, however, the hydrological models cannot handle some surface flow processes that are connected to the estuarine processes.

We first verify the robustness and stability of SCHISM with a realistic and challenging conservation test. A reservoir

of 2.5 km (L)  $\times$  5 km (W) (Fig. 1) is initially dry and starts to receive rainfall at the start of the simulation. The reservoir bed consists of 6 different linear slopes (ranging from  $10^{-3}$  to  $10^{-2}$ ) as shown in Fig. 1d, so we can examine the different flow responses there. The rainfall rate remains constant at 3 cm/h for half a day, followed by a linear decrease to 0 at the end of the 1st day, with no rain afterward (Fig. 2a). The change of the total volume of water from its initial value can be easily calculated analytically and compared with the modeled value.

The model horizontal grid consists of 7945 triangles with equivalent radii ranging from 46 to 80 m and an average radius of 49 m (Fig. 1c). Using the equivalent diameter as a measure for grid resolution, the average resolution of  $\sim 100$  m is similar to what we used for the Delaware Bay watershed. In the vertical dimension, we use 1 layer since 2DH mode is sufficient and efficient for such situations, and it is also more stable than the 3D mode in the inundation regime. In the Delaware Bay case, we take full advantage of the model polymorphism and use the 2DH mode in hydrological areas. Manning's  $n$  is set at a large value of 1, and other choices of parameters are consistent with the actual Delaware Bay case: a time step of 150 s, implicitness factor of 1, and the threshold depth of  $h_0 = 10^{-6}$  m for wetting and drying. A large roughness factor, together with the very small  $h_0$  used, leads to large bottom friction coefficients for the thin-layer flow of low Reynolds number (McKeon et al. 2004).

The mass conservation is first checked for this test. As shown in Fig. 2b, the modeled volume change closely tracks the analytical value throughout the 2-day simulation, with a maximum error of 1.2%. The total volume remains constant after the rain stops at  $t = 1$  day as expected. The modeled inundation sequence indicates that there is little “ponding” on the steeper slope in the north and a lot of ponding on the gentler slope in the west, as expected (Fig. 3). The impounded water slowly drains after the rain stops. As it will be shown later, the direct precipitation makes some differences to the total inundated area and also in the total water level in the rivers so it is important to have a model that is able to properly account for the pluvial effects.

### 2.3 Hydraulic jump

The bathymetric variations in upstream rivers and watershed are typically much more rapid than those in the coastal areas. Abrupt changes in depths are responsible for several important processes including flow discontinuity in the form of hydraulic jumps. Strictly speaking, some of these processes are non-hydrostatic in nature due to rapid acceleration in the vertical dimension. If our focus is on the impact of such processes on the larger scales, however, we can still use hydrostatic models to efficiently simulate the interactions between these and other processes.

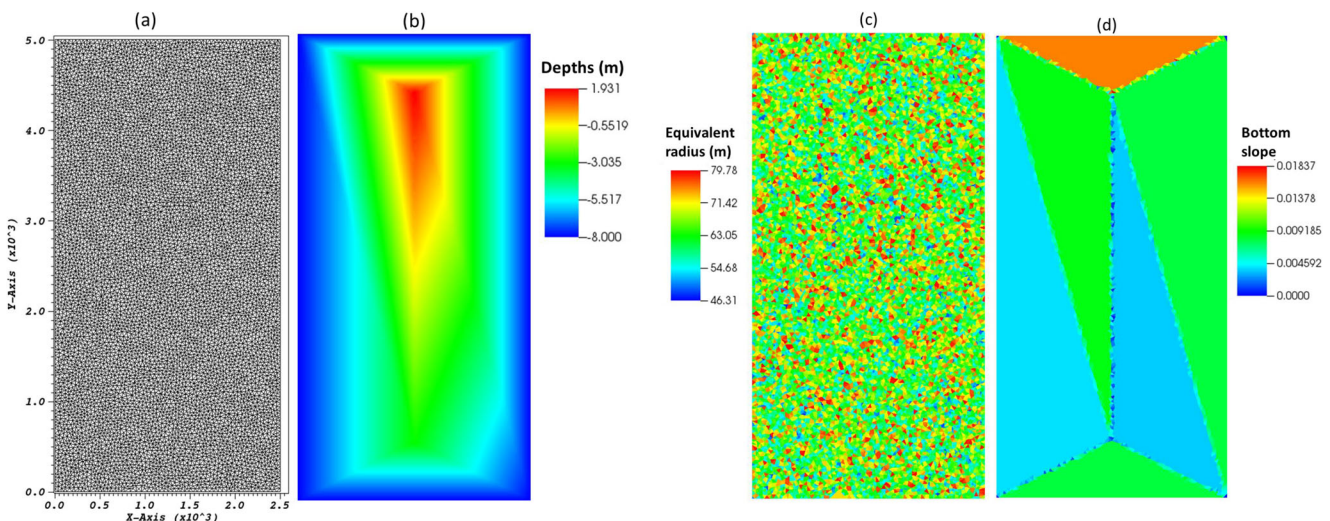


**Fig. 1** Domain and grid for the reservoir test. **a** Horizontal grid; **b** bathymetry; **c** grid resolution in the form of equivalent radius; **d** bottom slope

We test SCHISM's ability to simulate the hydraulic jump over a weir. The domain used is identical to case A in Stelling and Duinmeijer (2003), who presented an analytical solution under the hydrostatic assumption (Fig. 4). For this 2DV case, we use a rectangular flume of size  $100\text{ m (L)} \times 1\text{ m (W)} \times 1\text{ m (H)}$ , with a uniform horizontal resolution of  $0.5\text{ m}$ . In the middle of the flume, there is a weir with a slope of  $1:5$  on each side and a  $10\text{-m-long crest}$  (Fig. 4). In the vertical, we used 1 layer. The time step used for this lab scale case is  $0.1\text{ s}$ , and density variation is not included in the simulation. Initially, the still water surface is right at the crest of the weir and flow is injected from the left-hand boundary with a constant rate of  $1\text{ m}^2/\text{s}$  (per unit width), resulting in a depth-averaged velocity of  $1\text{ m/s}$ . On the right-hand boundary, the free surface is clamped at the initial elevation ( $0\text{ m}$ ). The model reached steady state within  $1\text{ h}$  and a hydraulic jump is fully developed downstream of the weir. The steady-state profile is shown in Fig. 4, which compares

well with the hydrostatic analytical solution. The main differences are found over the weir and in the jump; the modeled surface is not as sharp as the analytical solution due to inherent numerical diffusion, which was also present in most other models (Stelling and Duinmeijer 2003).

The test shown above is at a lab scale. To test the model performance in field scale applications, we test the model's sensitivity to grid resolution in a hydraulic jump situation in the upstream Delaware River. The domain used resembles the real case, with a rectangular box of  $4\text{ km (L)} \times 200\text{ m (W)} \times 5\text{ m (H)}$ . A single slope of  $1:100$  is resolved with 2,4,8 grid points, and the inflow rate is  $200\text{ m}^3/\text{s}$  and the downstream elevation is clamped at  $-0.8\text{ m}$  (which roughly corresponds to the field case depicted in Fig. 18 below). Other model parameters follow the model setup shown in Section 3.1 below. Note that there is no analytical solution for this case. The model results shown in Fig. 5 indicate that while the details of the jump differ (in particular, the jump is more developed

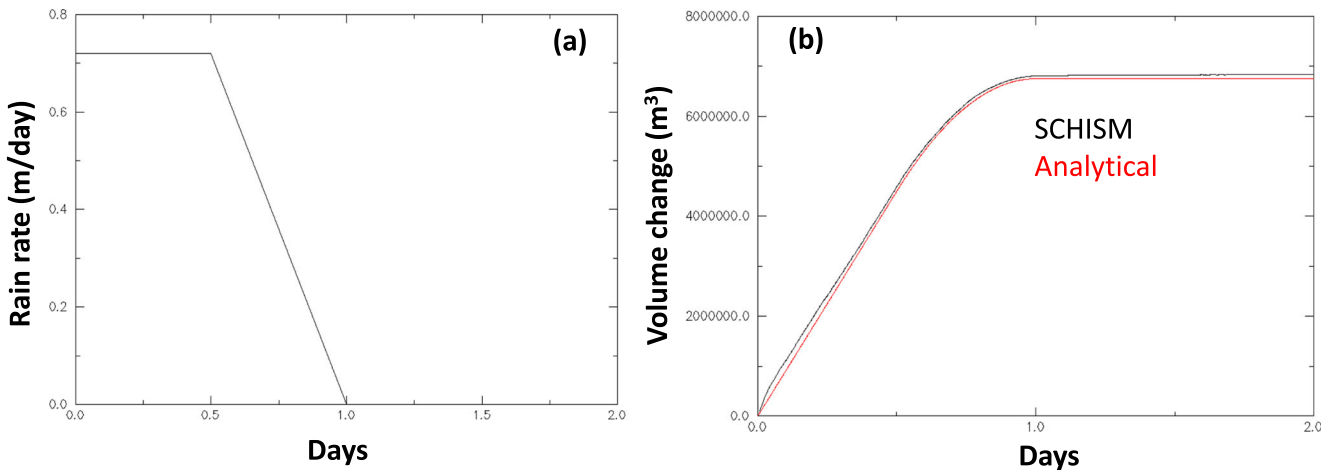


**Fig. 2** Time history of **a** rainfall rate and **b** volume change from the initial condition

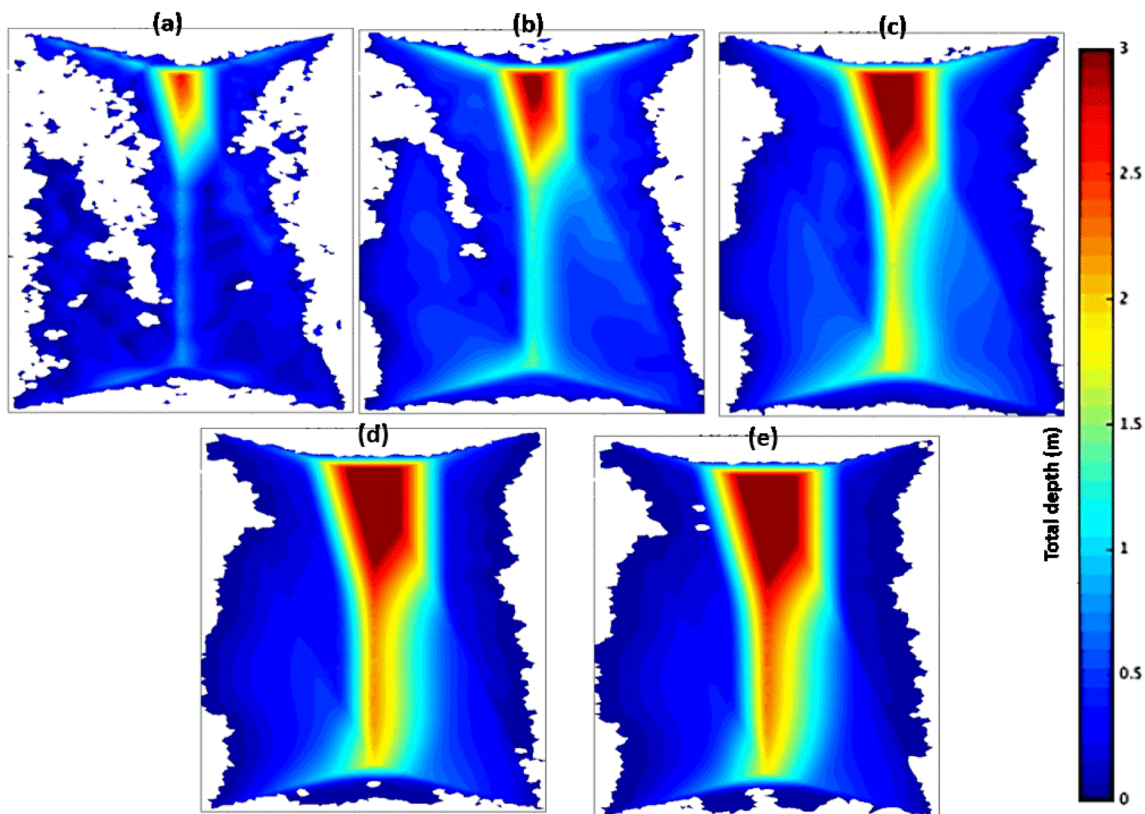


**Fig. 3** Snapshots of inundation depths at DD:HH:MM = **a** 00:04:50; **b** 00:13:50; **c** 01:00:24; **d** 01:15:00; **e** 02:00:00

under finer resolution), the modeled elevation at upstream is relatively insensitive to the grid resolution, and by virtue of mass conservation, the modeled velocities at up/downstream are also insensitive to the resolution choice. Therefore, if we do not care about the details of the jump but focus on larger-scale processes, coarser resolution is acceptable. In case finer resolution is warranted, locally high resolution can be readily enabled with our model grid; this is especially efficient in SCHISM as the time step needs not be reduced.

### 3 Compound flooding in Hurricane Irene: model validation

#### 3.1 Baseline model setup and sensitivity runs

A large UG is generated to cover the US East Coast and Gulf of Mexico, with finer resolution in the Delaware Bay (Fig. 6). The land boundary is cut at 10 m above MSL except for the Delaware River, where we extend the domain to the USGS gauge of Riegelsville, roughly at 40 m

**Fig. 4** Validation of SCHISM for hydraulic jump for a lab case

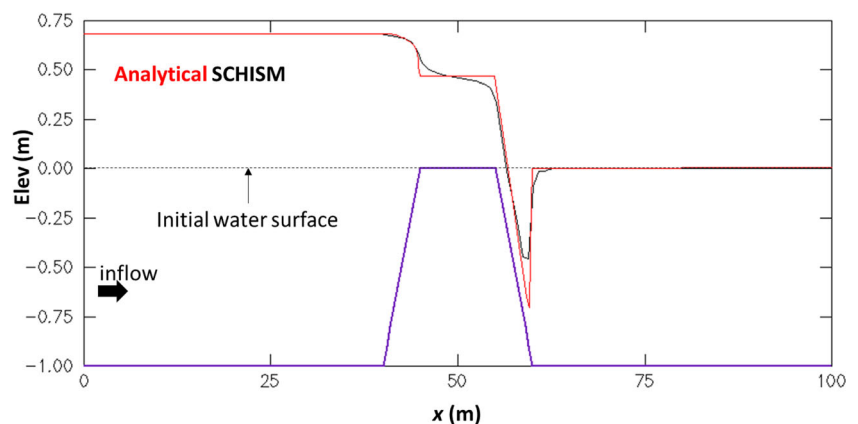


**Fig. 5** Hydraulic jump results for a domain based on Delaware River as a function of the grid resolution

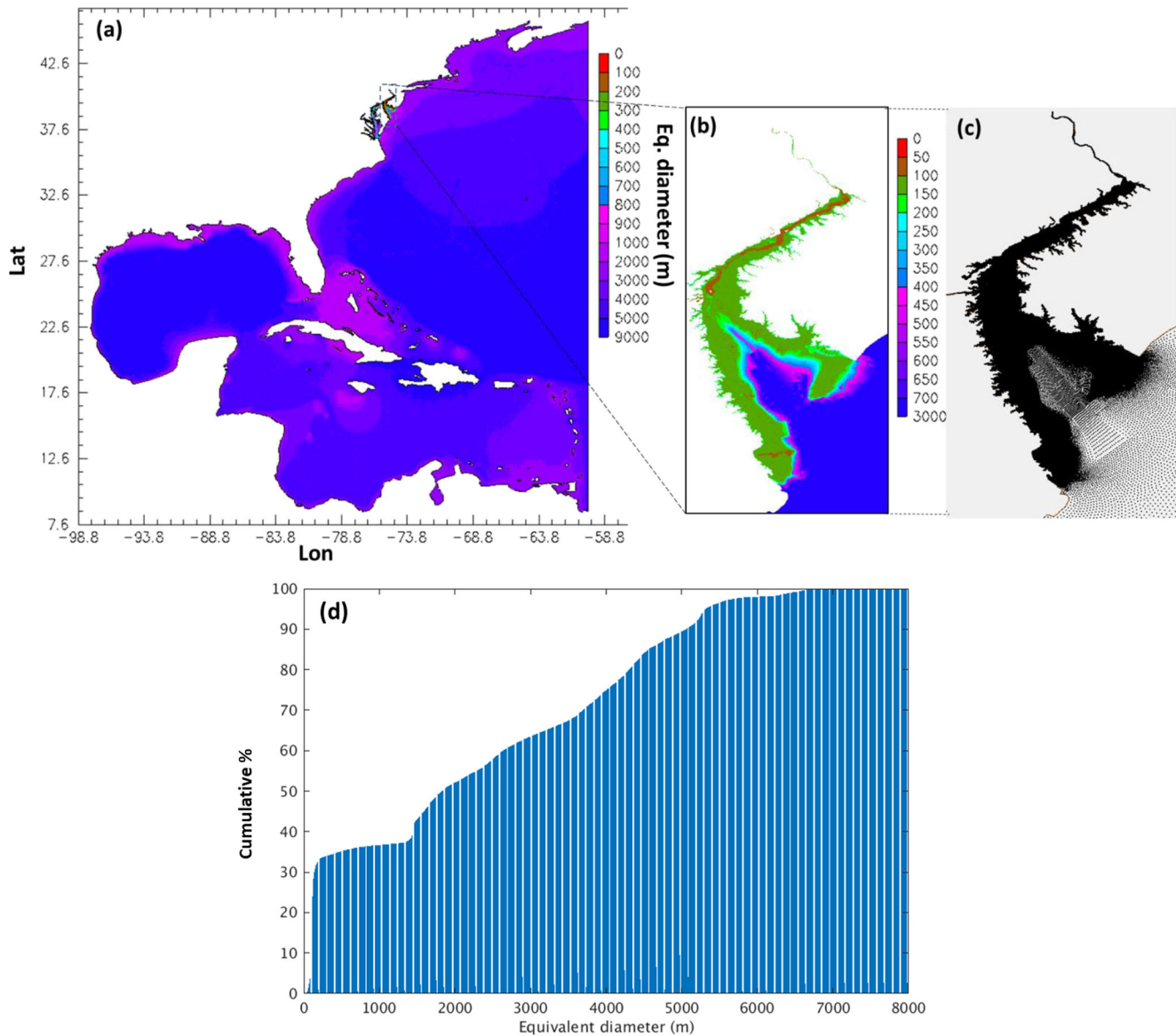
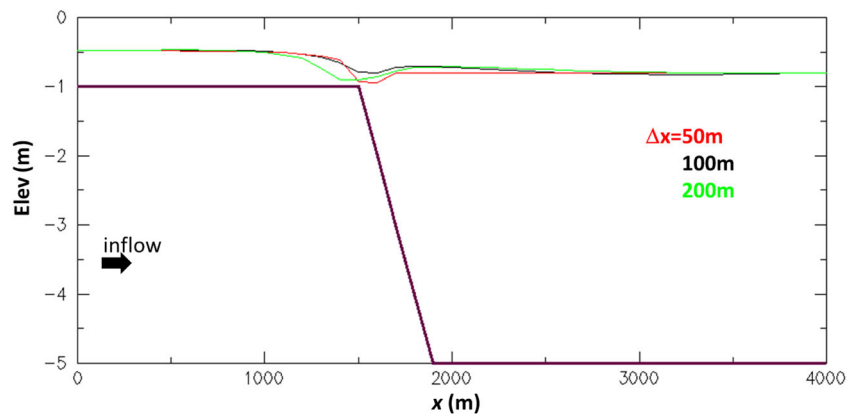


**Fig. 6** **a** Grid resolution in the form of equivalent diameter, and **b, c** zoom in around Delaware Bay. **d** Histogram of resolution. Only grid nodes are shown in **c** for clarity

**Table 1** Sensitivity runs used in this paper

Run name	Setup
baseline	3D baroclinic
2D	With a single vertical layer and a different bottom friction formulation (Manning's $n$ )
coarse_reso	Same as "baseline" but with ~300-m resolution in the watershed
base_precip	Same as "baseline" but with direct precipitation incorporated onto the surface layer
base_no_river	Same as "baseline" but with no coupling with NWM (no rivers or point sources)
base_no_storm	Same as "baseline" but with a maximum of 10 m/s for wind velocity

above MSL. The UG has 667 K nodes and 1273 K elements, including 39 K quadrangular elements used to represent the shipping channel. The grid generation process in SCHISM focuses on resolving important physical features (shelf break, channels, etc.), as the implicit scheme used alleviates the efficiency bottleneck associated with high resolution or skew elements. The average resolution in the grid is 1.7 km, with a mode of 232 m. As seen in Fig. 6d, ~30% of the cells have resolution finer than 140 m. A quasi-uniform triangular grid with a resolution of 6–7 km is applied in the open ocean, which is smoothly transitioned to about 2 km resolution near the coastline. Inside the Delaware Bay, we use a typical resolution of 600 m in the lower Bay channel, 50 m in the upper Bay channel, 150 m in the watershed areas above MSL, and down to 20 m in some small creeks. After the grid is generated, the digital elevation models (DEMs) are linearly interpolated onto the computational grid without any bathymetry smoothing. The DEMs we used include the global relief model ETOPO1 (Amante and Eakins 2009) for the ocean, and the 1-m USGS Coastal National Elevation Database (Danielson et al. 2018) for the Delaware Bay. For simplicity, we use a flat datum of NAVD88 for the entire domain and let the model set up the surface slope from downstream to upriver organically.

The vertical discretization used in the model is the hybrid terrain-following-like LSC<sup>2</sup> coordinate (Zhang et al. 2015), with variable number of layers at different depths. The average number of layers is 18.3, with maximum of 44 layers in the deepest ocean and only 1 layer for areas with depths shallower than 0.5 m. As a result, 2D representation is applied in 30% of all grid elements. The wetting and

drying threshold is set at  $h_0 = 10^{-6}$  m; such a small threshold is needed to accurately capture the very thin layer of fluid initially formed on dry land during precipitation events (cf. Section 2.2); the use of larger values for  $h_0$  would lead to underestimation of inundation because initially the fluid depth is very thin (e.g., with a moderate rainfall rate of 1 in./day, the amount of water fallen on dry elements within a time step would only be 0.044 mm) and so, the grid elements on dry land would have never become inundated. The model is stable even with this choice of small threshold for wetting and drying, courtesy of the implicit scheme.

One of the key calibration parameters is the bottom friction. Through calibration, we set a spatially variable bottom roughness: 0.5 mm in the ocean and the lower Delaware Bay, and then linearly transitioned it to 0.05 mm in the mid- and upper Bay along the main channel; in the upland areas (3 m above MSL), we used a uniformly larger 1-mm roughness. Increasing the roughness factor in the upland areas to 1 cm led to essentially the same results. The surface stress is calculated from the bulk aerodynamic model of Zeng et al. (1998) using the atmospheric forcing from two ECMWF datasets, one with 30-km resolution (<https://www.ecmwf.int/en/forecasts/datasets/reanalysis-datasets/era5>, last accessed in June 2019) and the other with 9-km resolution (Magnusson et al. 2014). The initial condition and the non-tidal components of the boundary conditions are derived from HYCOM 1/12 reanalysis product ([hycom.org](http://hycom.org), last accessed in June 2019), and the tidal components of the boundary conditions (for elevation and horizontal velocity) are derived from FES2014 (Carrere et al.

**Table 2** Computational performance for different types of simulations. Note that both SciClone and Pleiades have multiple subclusters

Type	2D	baseline	coarse_reso	base_precip	base_no_river	base_no_storm
Grid nodes	667 K	667 K	527 K	667 K	667 K	667 K
Averaged vertical layers	1	18.3	18.3	18.3	18.3	18.3
Cluster	SciClone	Pleiades	SciClone	Comet	Pleiades	Pleiades
Cores used	72 (9 × 8)	1440 (72 × 2-0)	360 (18 × 20)	960 (40 × 24)	1400 (50 × 28)	1600 (100 × 16)
Real-time ratio	228	80	28	33	84	83

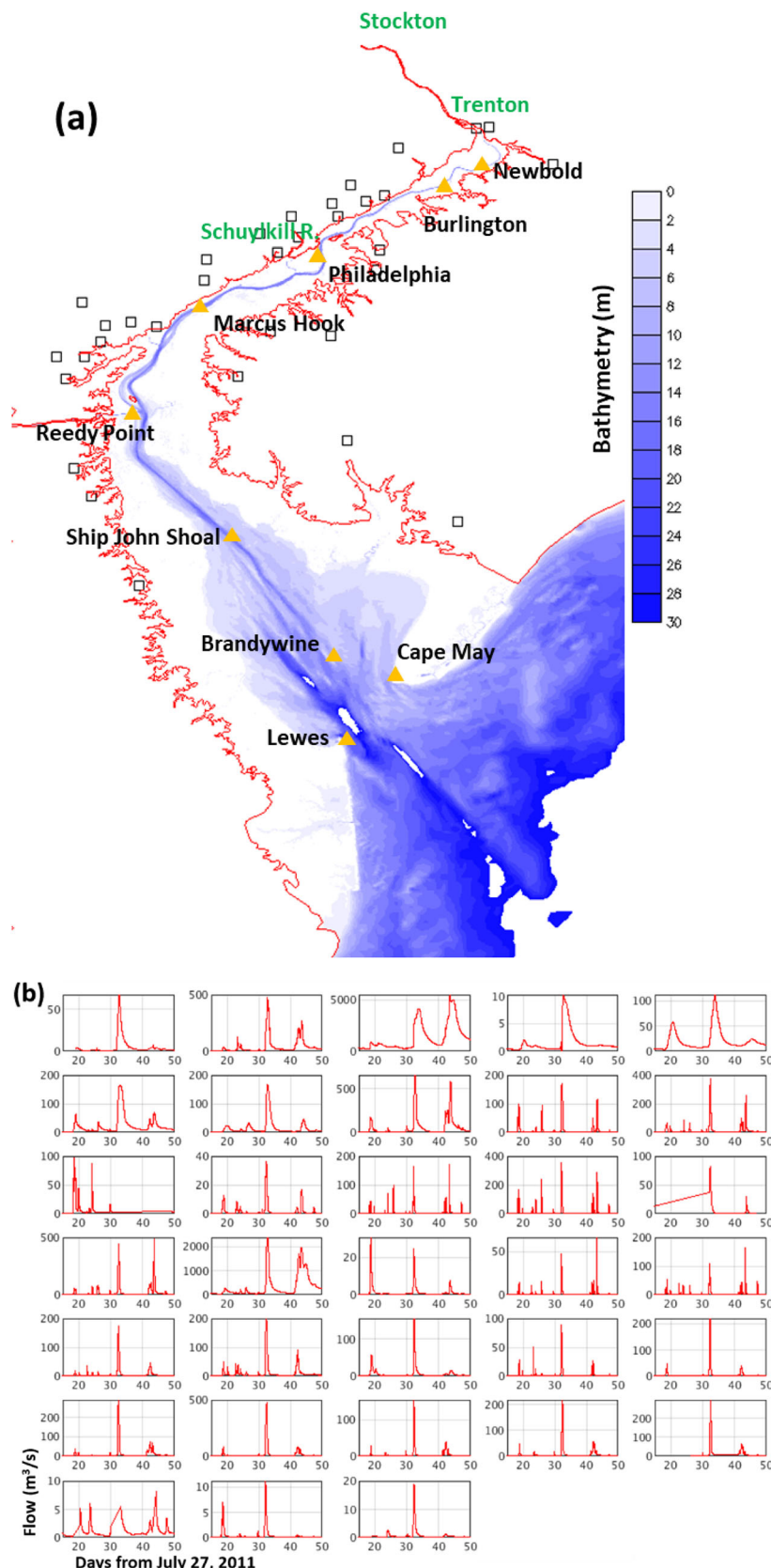


**Fig. 7** **a** USGS (squares) and NOAA (triangles) stations in Delaware Bay; **b** USGS observed flows at multiple river gauges (squares in **a**). Most of USGS gauges that reported flow data during Irene are outside our model domain due to the choice of the boundary at 10 m above sea level

2016). The river flows as predicted by NWM are injected into SCHISM domain along the entire boundary inside the Bay (~ 10 m above MSL); note that the model is able to handle the wetting and drying on such high ground as evidenced by the test in Section 2.2. We have not incorporated any feedback from SCHISM to NWM, so only one-way coupling is used here.

The model uses a non-split time step of 150 s. A bi-harmonic viscosity was added to the horizontal momentum equation (Zhang et al. 2016) to control the spurious inertial modes that often arise in large-scale UG models (Le Roux et al. 2005; Danilov 2012). In addition, a Laplacian viscosity in the form of Shapiro filter (Shapiro 1970; Zhang et al. 2016) is locally added near steep bathymetric slopes, where spurious modes would otherwise be exacerbated by the pressure gradient errors. A third-order WENO transport scheme (Ye et al. 2019) is used for tracer transport. The vertical viscosity and diffusivity are calculated by the generic length scale model ( $k \cdot k_l$ ; Umlauf and Burchard 2003). The simulation period starts on July 27, 2011 (i.e., 1 month before Irene's landfall on the US East Coast), providing sufficient time for spin-up because the initial conditions are from the fully dynamic conditions provided by the data assimilated HYCOM product. The simulation covers 50 days that include the main surge and the subsequent river flooding events.

Numerous sensitivity tests are also conducted based on the abovementioned baseline setup for analysis purpose, and results from some of these tests will be presented in

Section 4. Table 1 shows the sensitivity runs used in this paper; these runs explore the influence on the model results from 3D effects, grid resolution used in the hydrological regime, river flows, direct precipitation inside the model domain, and backwater effect from coastal processes.

The baseline setup achieves a performance of ~ 80 times faster than real time, using 1440 cores of NASA's Pleiades. The 2D model runs approximately 57 times faster than the baseline and can be efficiently conducted using as few as 40 cores. More detailed information on model's computational performance is shown in Table 2.

### 3.2 Model validation

The model skill at the Bay stations has been reported elsewhere (Ye et al. 2020), and so, only a brief summary is presented here. The average mean absolute error (MAE) and correlation coefficient for the elevation are 13 cm and 0.98 respectively. The average MAE and correlation coefficient for salinity are 0.86 PSU and 0.77 respectively. Comparison of elevation at three NOAA stations in lower, mid-, and upper Bay (the locations of which are shown in Fig. 7a) is shown in Fig. 8; also included are model results from the 2D SCHISM. As shown in Fig. 8b, c, the effects of baroclinicity, mostly due to the Gulf Stream, are significant during the restoration phase and account for ~ 14% of the difference (Ye et al. 2020). Overall, the model is able to simulate well the 3D processes that occur in the Bay during and after the main surge (Ye et al. 2020). The

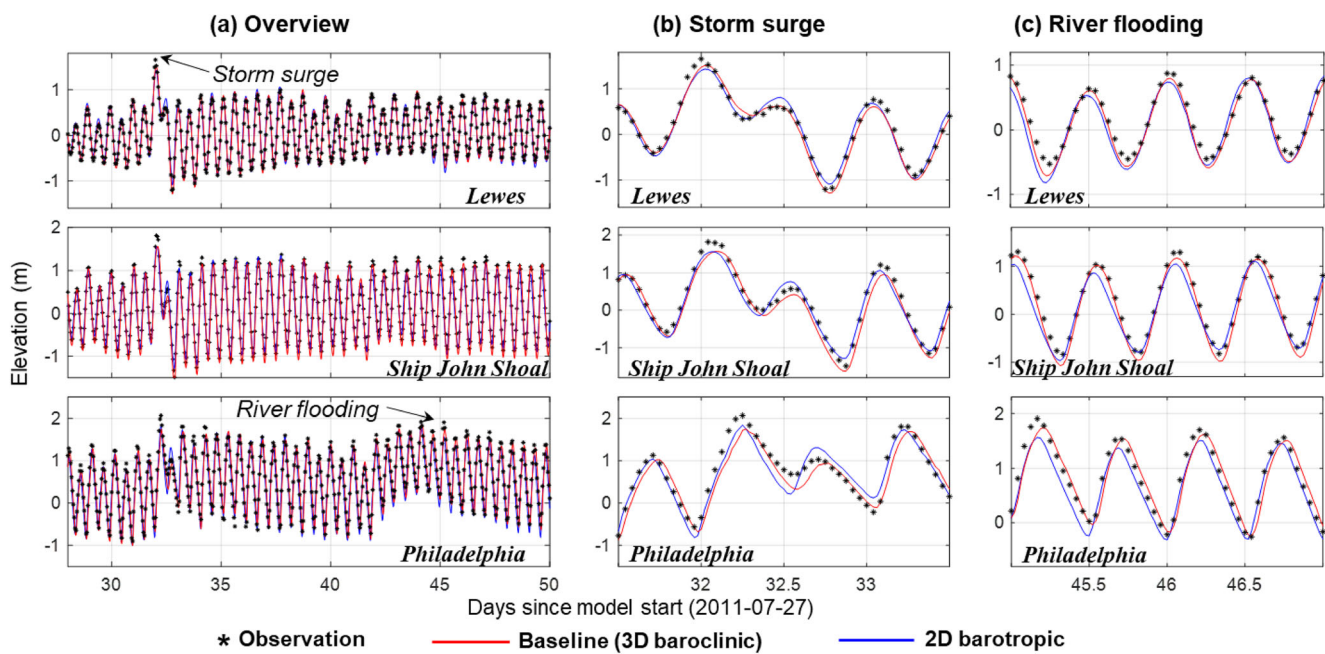


**Fig. 8** Comparison of elevations at 3 NOAA stations (see Fig. 7a for station locations). **b** and **c** show the details in the surge and river flooding periods. The elevations are relative to NAVD88

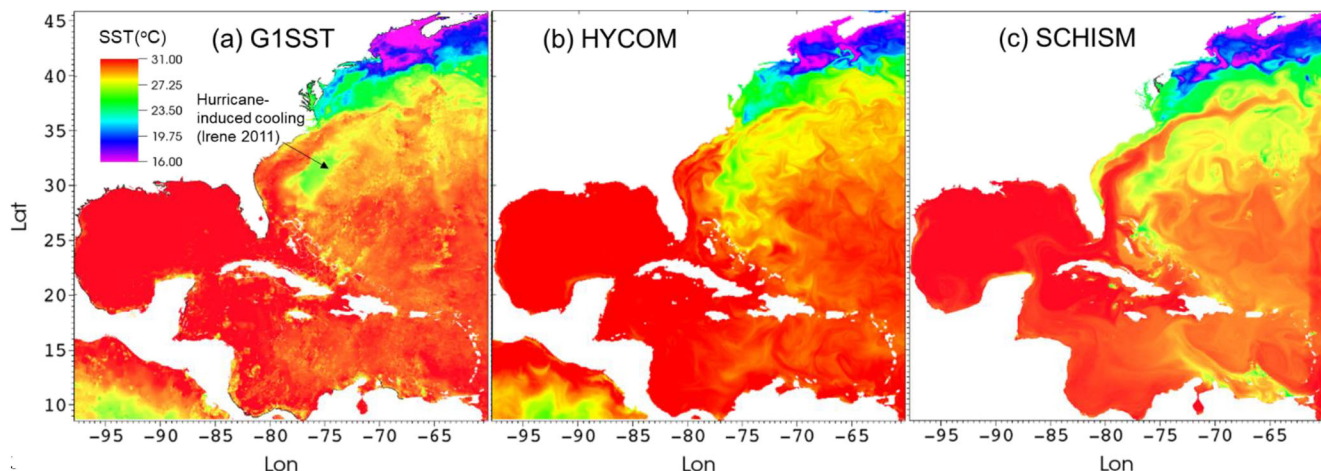


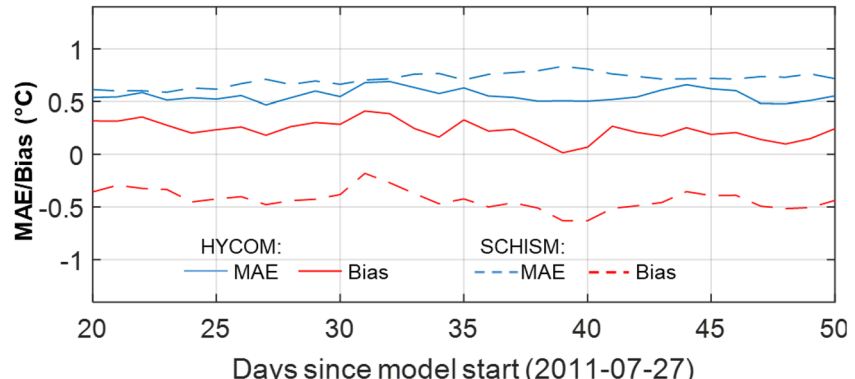
**Fig. 9** Comparison of SST on August 29, 2011

2D model generally yields a mean bias in the water level especially after the main surge (Fig. 8b, c), due to the absence of Gulf Stream (Ye et al. 2020). However, the 2D model is largely adequate for the hydrological processes and even the baseline 3D setup uses 2D mode in the watershed; for the sake of consistency, we will continue to use the 3D baroclinic baseline model setup for the remainder of this paper. The main advantage of this approach is the use of a single model to account for both 2D and 3D processes in the ocean and watershed.

Model skill for the large-scale baroclinic processes is assessed in terms of sea surface temperature (SST) and compared with the data assimilated product HYCOM in Fig. 9. The comparison is done a few days into the storm and the signature of Irene can be clearly seen, which is captured by both HYCOM and SCHISM. Both models also capture the interruption of the Gulf Stream by the storm, but the details of meanders and filaments differ from each other and from the satellite product. Over the entire domain, HYCOM has a lower MAE and a positive bias, while SCHISM has a larger MAE and a negative bias (Fig. 10). Sensitivity test results suggest that adjusting water type and albedo locally can further improve the SCHISM results but for the sake of simplicity, this is not pursued here.

The focus in this paper is in the hydrological regime. We first validate the model for the streamflow and river stages (elevations) in upstream rivers, including the Delaware River (upstream of the fall line of the Delaware Bay) and Schuylkill River (the 2nd largest tributary to the Bay). During the simulation period, two major flood peaks are observed by many USGS gauges in most rivers and creeks in the Delaware Bay watershed (Fig. 7b). The first peak roughly coincides with the landfall of Irene and the second peak occurs about 2 weeks after the main storm event (Fig. 7b). SCHISM captures both peaks as well as a couple of minor peaks well in both rivers (Figs. 11a and 12). The close agreement between SCHISM and NWM predicted flows is not surprising, since the boundary flow of SCHISM is derived from NWM; this agreement also confirms the volume conservation in SCHISM. Some minor differences exist between the two models especially in the phase of the floods in the Delaware River, suggesting that the flow (and other variables) is advected at slightly different speeds in the two models and in the observation. Note that NWM is still evolving as of this writing; although the NWM product used here is a reanalysis product, some small mismatches from observation (including phase errors of flood peaks)

**Fig. 10** Time history of MAE and bias in SST (over entire SCHISM domain) simulated by HYCOM and SCHISM



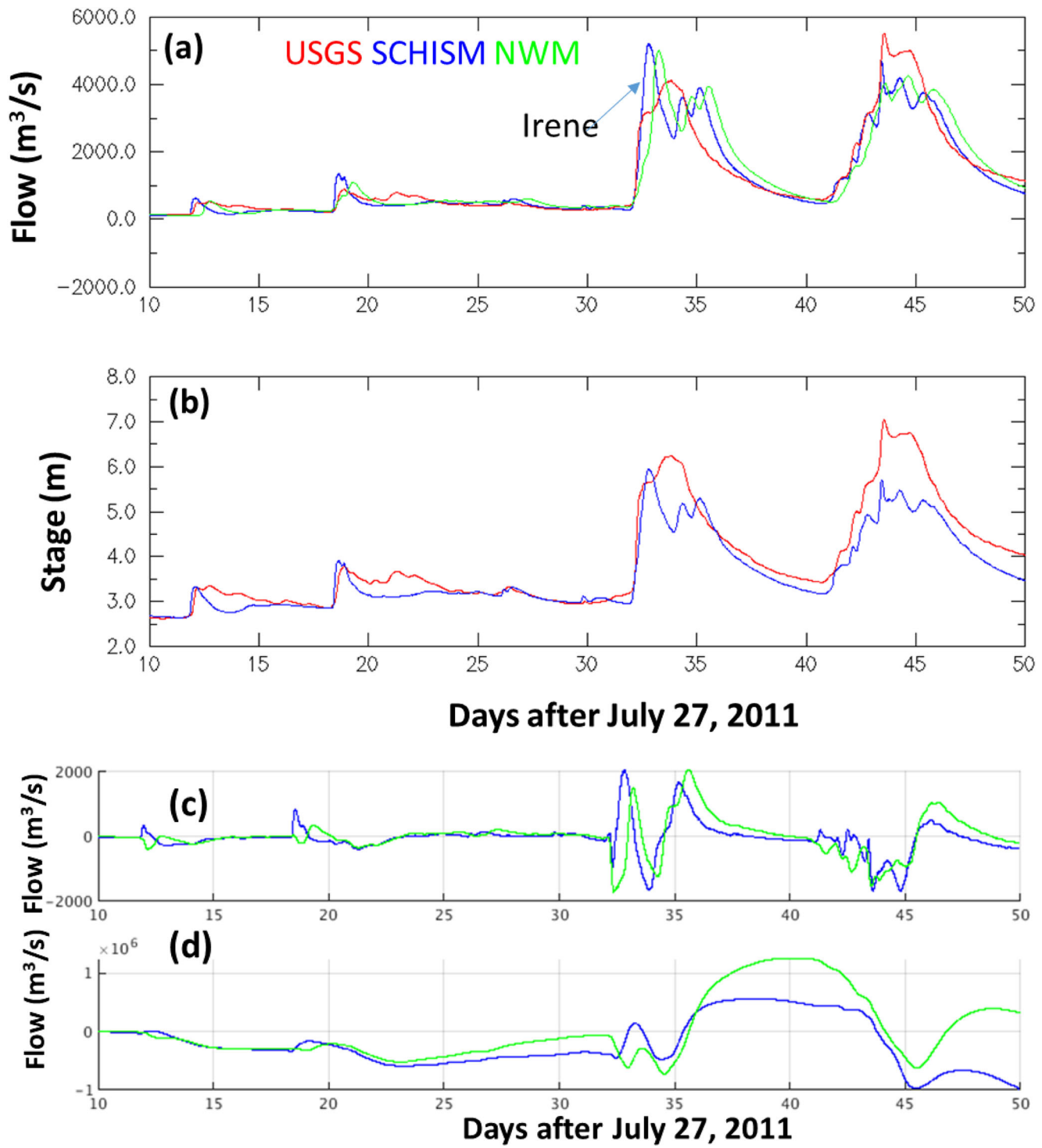


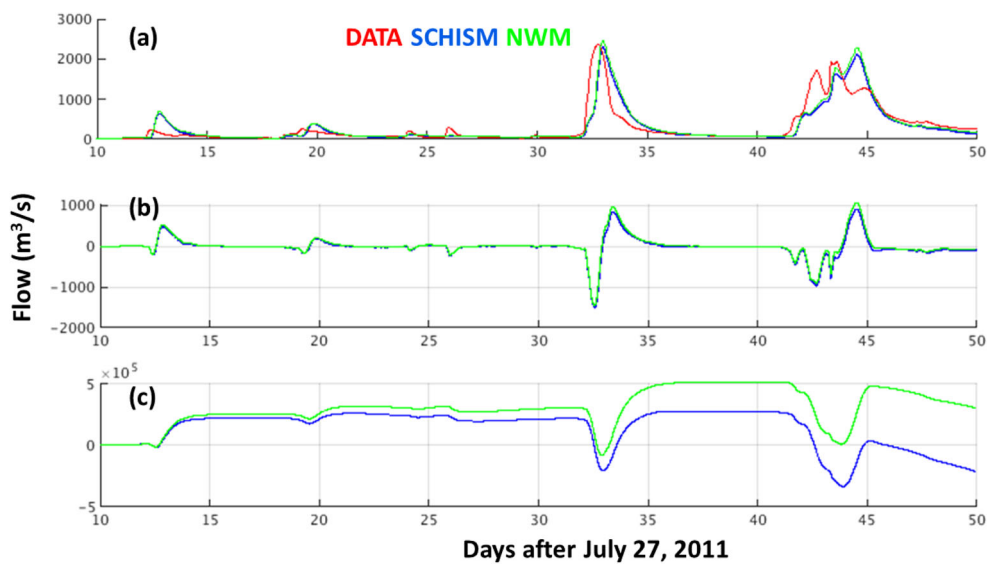
**Fig. 11** Comparisons of **a** streamflow and **b** river stage at the USGS station Trenton. Note that NWM does not provide stage information and the observed stage has been converted to NAVD88 using the datum

adjustment at the NOAA's Philadelphia station, but the adjustment is small (0.118 m) compared with the mean stage. **c, d** Flow errors and cumulative errors from SCHISM and NWM respectively

can be seen in Figs. 11a and 12. For example, the observed flow at Trenton indicates that the second peak (due to river flooding) is actually higher than the first peak (due to storm surge), whereas the NWM flow shows that the two peaks are generally similar with the first

being slightly higher. This wrong prediction of trend is directly translated into the SCHISM's flow in Fig. 11a, which may also account for part of the elevation errors at some downstream Bay stations. More importantly, the wrong trend is also apparent in the predicted elevation at

**Fig. 12** **a** Comparisons of flow at USGS gauge of Schuylkill River. **b, c** Flow errors and cumulative errors for SCHISM and NWM respectively



the same station (Fig. 11b). The errors in predicted flow show no clear biases in either model (Figs. 11c and 12b) and so the total runoff volume predicted by either model remains close to the observation, as evidenced by the cumulative volume error plots in Figs. 11d and 12c. Overall, the agreement with observed flow and elevation/stage is good (with MAE of 0.32 m for elevation (or 7% of the mean stage) and 254.8 m<sup>3</sup>/s for flow at the two stations), which confirms that SCHISM can realistically capture fluvial processes. The agreement of elevation at Trenton is even more remarkable given the uncertainties of the DEM used in upstream rivers. Note that a common flat datum (NAVD88) is used in the model and still the model is able to correctly set up the surface slope from ocean to upstream river. As can be seen in Fig. 11b, the mean surface elevation at Trenton during non-flood period is now ~3 m above that at the coastal stations like Lewes.

Further upstream of Trenton, the model uncertainty becomes larger, mainly due to the uncertainty in the DEM. The information given at the USGS gauge at Stockton indicates

that the average water surface is ~17 m above that at the coastal stations (Fig. 13). Unfortunately, it did not specify the local bottom elevation so we could not verify the DEM error or compare the total water level there. The computed surface elevation at this gauge is ~1 m higher than the observation (Fig. 13). Note that the observation is given with respect to NGVD29, whereas the modeled elevation used NAVD88 and the conversion method between the two datums is not clear at this far upstream gauge. However, if we focus on the surges alone, with a constant adjustment in the vertical datum, it is encouraging to see that the model is able to capture the multiple river surges reasonably well (blue curve in Fig. 13). The results here highlight the importance of addressing the uncertainties in the shallow water bathymetry and of properly accounting for the differences in various vertical datums used. Recent advancement in remote-sensing technology (e.g., ground base water penetrating Lidar) is likely to bring breakthrough to these remaining challenges and make the model predictions more reliable in upstream rivers. Overall, our model results are very encouraging and represent a major

**Fig. 13** Comparisons of stage at USGS gauge of Stockton. Note that the vertical datums used in the observation and model are NGVD29 and NAVD88 respectively

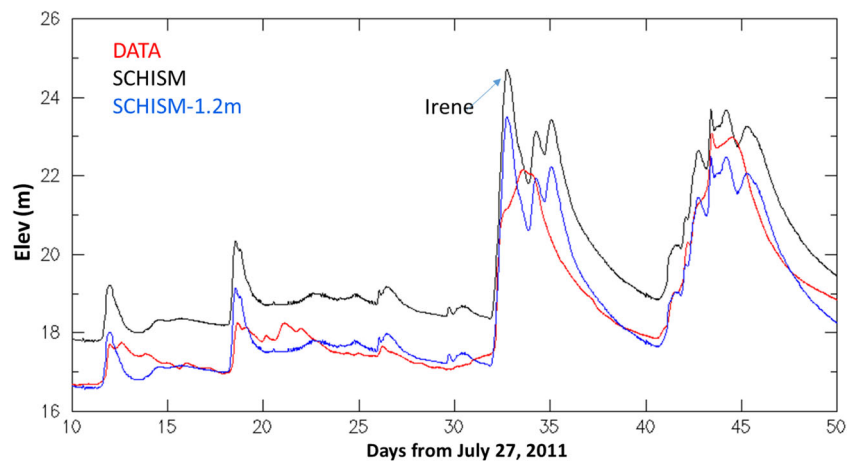
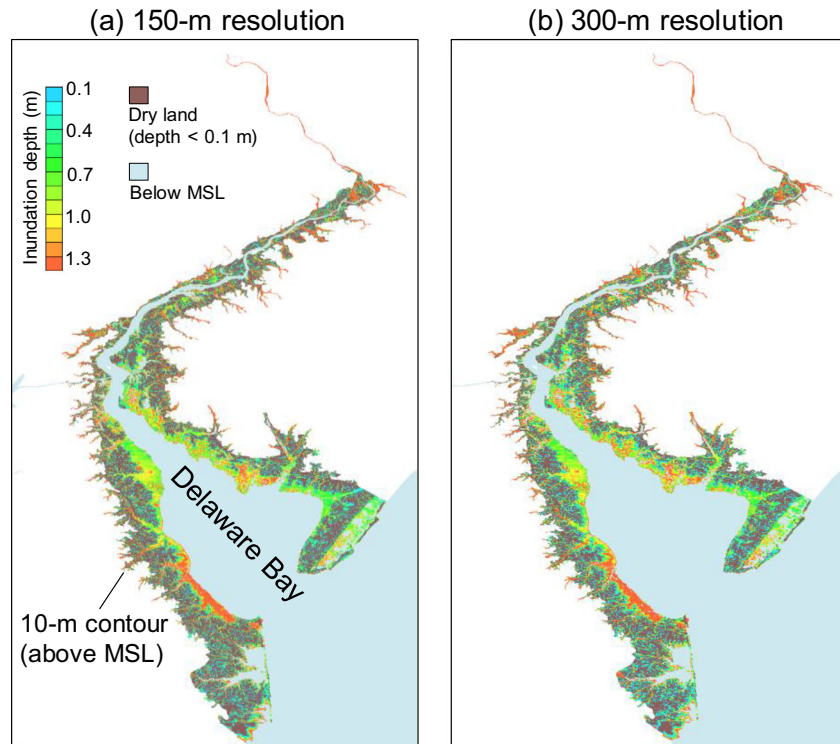


**Fig. 14** Comparison of the maximum inundation depths between two grid resolutions: **a** baseline, 150-m resolution in the watershed above MSL; **b** sensitivity run with a 300-m resolution in the watershed above MSL



step for a hydrodynamic model to simulate the hydrological regime, a critical step toward a fully coupled hydrologic-hydrodynamic modeling system (Santiago-Collazo et al. 2019).

#### 4 Discussions

Compound flooding by definition involves multiple processes and their interactions. Therefore, it is important to assess the

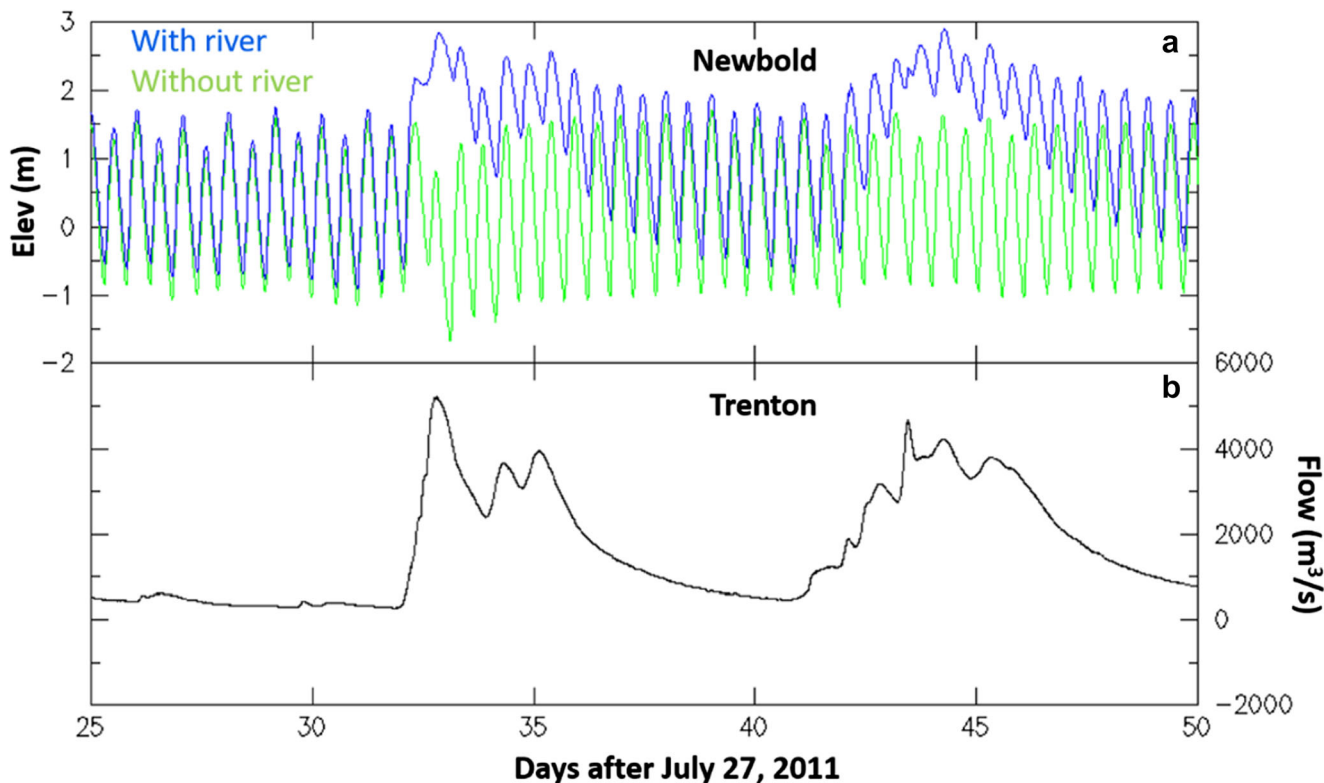


**Fig. 15** River influence as seen at **a** Newbold. The influence becomes significant after the storm with the incoming river floods as can be seen from the **b** Trenton flow from NWM

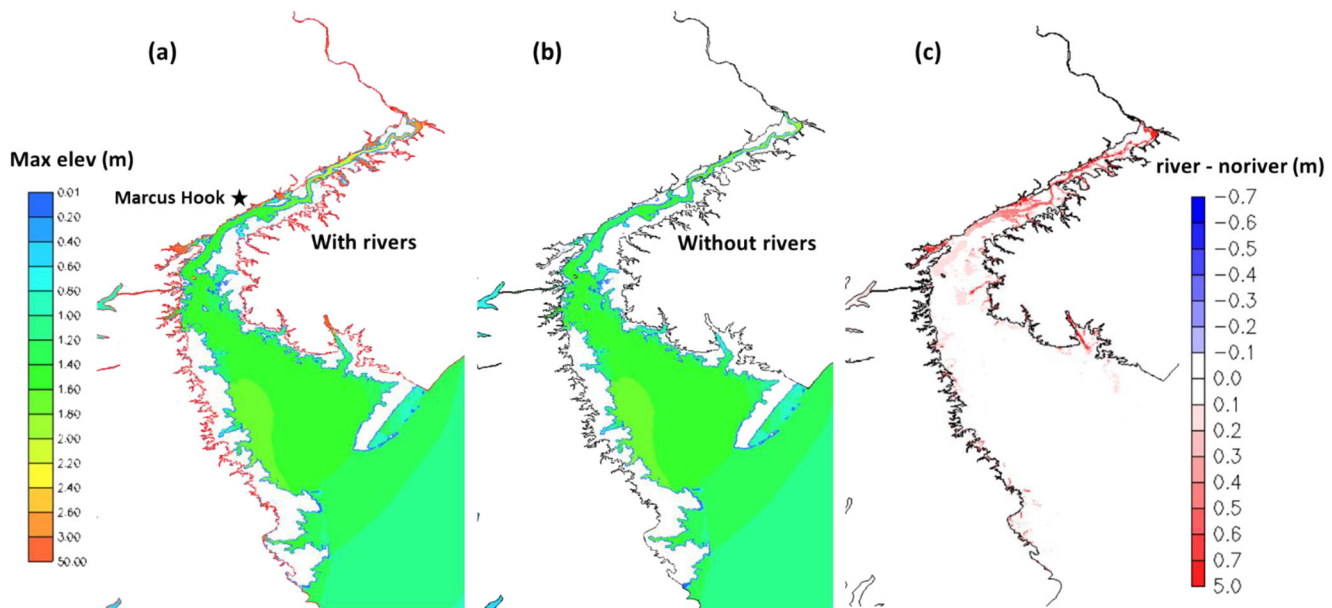


**Fig. 16** The effect of rivers in the maximum elevation during the simulation period: **a** with streamflow inputs from NWM; **b** without streamflow inputs; **c** the difference between **a** and **b**. To avoid ambiguity of elevation at dry instances, the total water depths are used to calculate the difference in **c**

relative roles of these processes and to understand the mechanism of their interactions. In this section, we will conduct sensitivity tests (cf. Table 1) to provide insights into various mechanisms that are at play during such events. A major goal for this section is to assess the adequacy of the current strategy of using a one-way coupling approach between NWM and SCHISM in the presence of the backwater effects.

#### 4.1 Grid sensitivity

An important practical consideration for simulating the compound flooding events is the grid resolution required. Since the simulation covers a large domain and the hydrological

regime generally requires adequate resolution, it is important to use appropriate resolution for efficiency purpose. This is especially important when we extend the same model to cover all estuaries of entire East Coast and Gulf of Mexico.

The grid resolution used in the areas above MSL is mostly  $\sim 150$  m in the baseline. Coarsening this to  $\sim 300$  m reduces the grid size by 21%, which represents a considerable amount of saving. The calculated inundation depths from the 300-m resolution are compared with those from the baseline in the watershed area (above MSL) in Fig. 14. Only some minor differences are observed; in particular, the total inundated areas in the watershed are only reduced by 0.2% with the coarser 300-m resolution. As our main focus is to study the interaction between hydrological and hydrodynamic processes, this difference can be neglected.

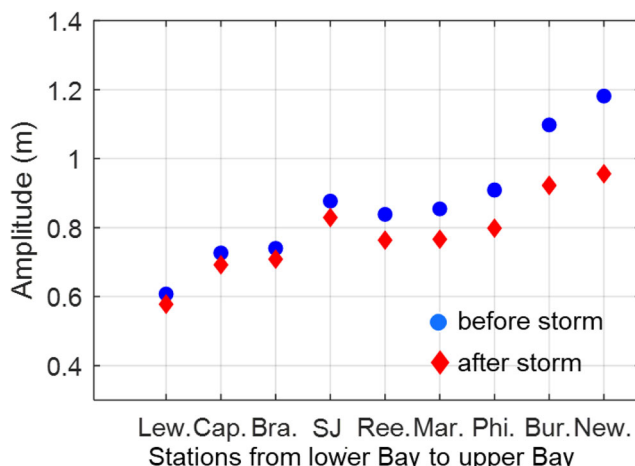


**Fig. 17** Non-stationary M2 amplitudes as shown by harmonic analysis for two 20-day periods: before storm (August 7–27) under normal conditions and after storm (September 15–October 5) under the influence of river flooding

#### 4.2 River influence

The influence from rivers during storm surges has not been carefully studied before. This influence is expected to be significant at locations closer to the rivers (i.e. upper Bay), especially if river flooding accompanies the storm as in the case of Hurricane Irene. Figure 15 compares the elevations at the most upstream NOAA station, calculated with and without inflows from NWM. The difference is striking almost immediately after the storm, with the arrival of first flood peak as seen from the nearby Trenton gauge. Moreover, the elevated surface stays high for more than 2 weeks after Irene has left the region, sustained by the continued large flow and the 2nd flood that arrived  $\sim 10$  days later (Fig. 15). Obviously, the river influence

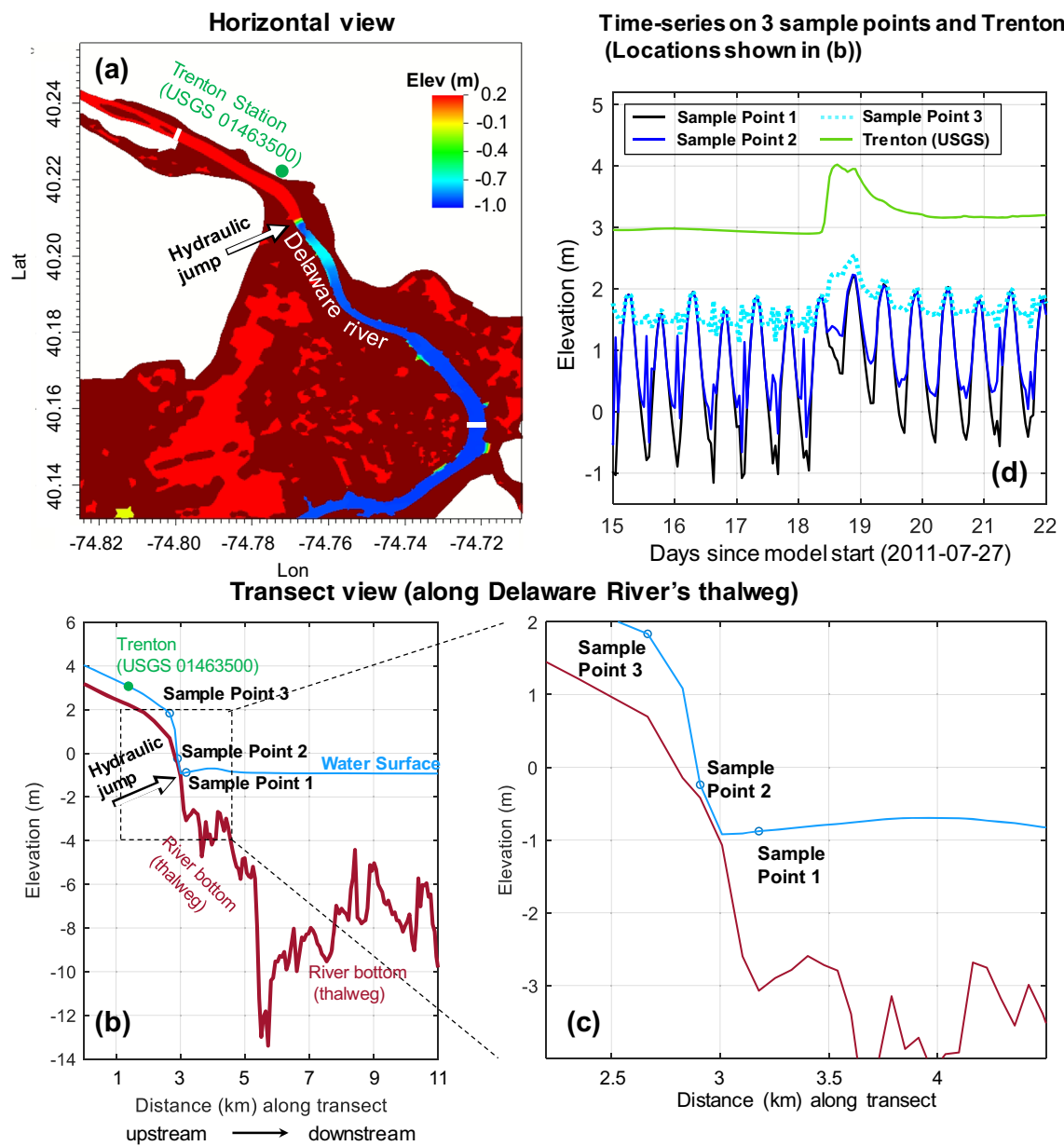


**Fig. 18** Hydraulic jump in Delaware River. **a** Snapshot of surface elevation showing a discontinuity; **b** side view of the hydraulic jump near an abrupt change of bathymetry along the thalweg; **c** zoom in view

of **b**; **d** time series of elevation at 4 points along the thalweg (3 sample points plus USGS gauge Trenton, locations shown in **b**), indicating the diminishing of tides upstream

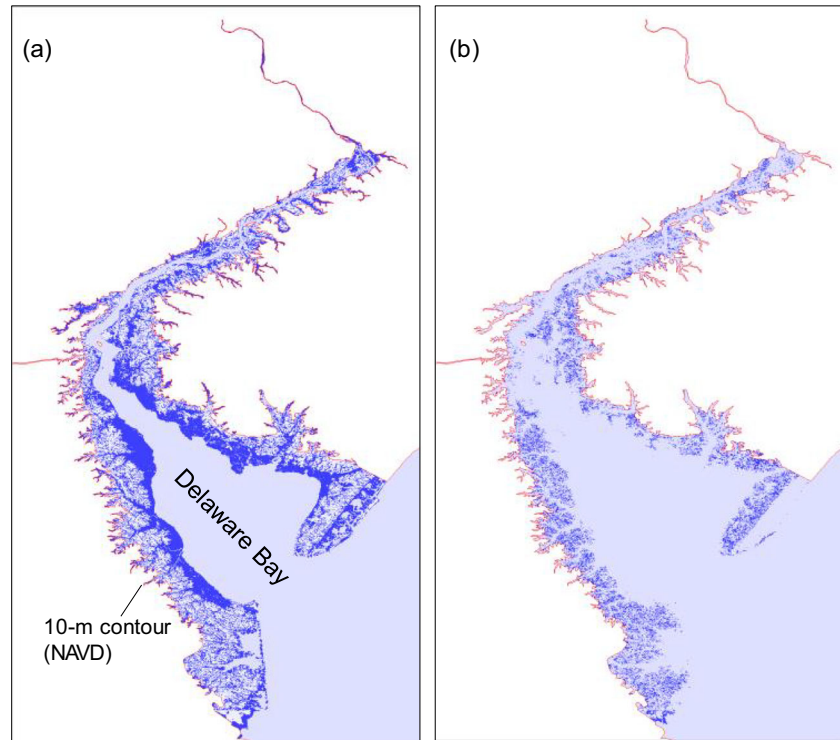
is very pronounced at this station; in fact, the storm-induced surge is smaller than that from the river flood at this station.

To examine how far the river influence propagates into the Bay, we compared the maximum elevations calculated with and without rivers. The wetting and drying can lead to misleading results as the surface elevations at dry instances are not well defined, and the issue is particularly severe at very high ground (e.g., upstream Delaware River). Therefore, when calculating the differences in elevations, we opt to use the total water depths, as the latter are well defined at dry instances (i.e., 0 m), and the difference between the total water depths is equal to that between the surface elevations (assuming the same bottom elevation).

Figure 16 indicates that the rivers generally help push the elevations higher in the region upstream of Marcus Hook. The relatively narrow channel upstream of Marcus Hook helps accentuate the river influence in the upper Bay (Fig. 16).

Rivers are known to influence tidal propagation as well. For example, tides can become non-stationary in large rivers (e.g., Columbia River; Jay and Flinchem 1999). The situation is found to be similar in the Delaware River. As shown in Fig. 17, the tidal amplitudes in the Bay increase from lower to mid Bay, then slightly decrease around the place where the channel turns before increasing again upstream. The trend is the result of the combined effects of bottom friction, channel constriction, and

**Fig. 19** **a** Inundated area (darker blue) in the Delaware Bay watershed (above MSL) during the entire simulated period from baseline (without precipitation); **b** additional inundated areas after including precipitation in the atmospheric forcing



meandering (Jay 1991; Lanzoni and Seminara 1998). While the M2 tidal amplitudes are similar during a non-flood and a flood period in the lower and mid Bay, the amplitudes are quite different in the upper Bay. Interestingly, the “regions of influence” by rivers for tide (Fig. 17) and surges (Fig. 16) approximately agree with each other. The results demonstrate that as the tides propagate into the narrow channel of the upper Bay, they become increasingly nonlinear and distorted by rivers (Kukulka and Jay 2003a, b; Moftakhi et al. 2013).

The Delaware River also serves as a barrier for tidal propagation upstream. An abrupt transition in bathymetry that resembles a weir is located ~ 2.7 km downstream of the Trenton gauge, where a hydraulic jump is usually observed (Fig. 18). The location of this “weir” roughly represents the head of tide, as the tides are effectively damped out a short distance (~ 0.5 km) upstream of the weir (Fig. 18d).

The results here confirm the importance of including the river influence in storm surge simulations as described by others (e.g., Dresback et al. 2013), and a seamless model that traverses different regimes is obviously advantageous in simulating this type of nonlinear interactions. Besides large rivers

(such as Delaware River), smaller rivers and creeks may also exert some local influence (e.g., flash flood as shown in the section below).

#### 4.3 Precipitation effects

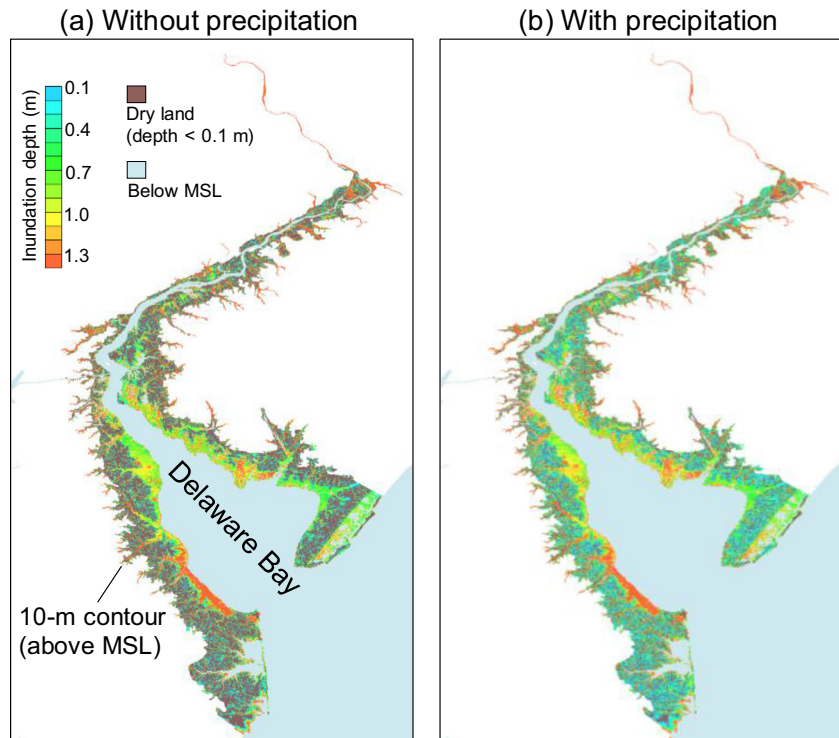
In traditional estuarine and coastal model applications, direct precipitation onto the water surface is often neglected in the volume budget. However, since the current model domain includes a portion of the watershed, the effect of direct precipitation on the inundation pattern on the upland and the elevations at upper Bay stations needs to be carefully examined. This is especially important because some heavy precipitation as large as 10 in./day occurred during Hurricane Irene.

In this analysis, we neglect the interaction between surface and groundwater for simplicity. We define the cumulative inundation area as the sum of areas of all elements with water depth exceeding a given threshold (0.1 m, a commonly used threshold for “nuisance flooding” (Moftakhi et al. 2018); note that the same wetting and drying threshold of  $10^{-6}$  m was used in the simulation) at any time during the 50-day simulation period. The baseline results (without precipitation; Fig. 19a and Table 3) indicate that about 55% of the Delaware Bay watershed (defined here as the areas above MSL) is inundated. The inundation is the direct result of the streamflow injected along the model’s land boundary as provided by NWM. The sensitivity results with direct precipitation added show a significant response from pluvial processes, i.e., a 19% increase in the inundated area, or extra 692 km<sup>2</sup> (Table 3). The

**Table 3** Inundated area in the Delaware Bay watershed (above the MSL) through the entire simulation period. The percentages are calculated with respect to the total watershed area

	Inundated area (km <sup>2</sup> )	Percentage inundated area (%)
Without Precip.	2034	55
With Precip.	2726	74

**Fig. 20** Maximum inundation depths in the Delaware Bay watershed (above MSL) during the entire simulated period: **a** “baseline,” without precipitation; **b** “base\_precip,” including precipitation in the atmospheric forcing. The burgundy areas have depths less than 0.1 m and are considered less hazardous



locations of the additionally inundated areas are widespread throughout the watershed as shown in Fig. 19b. The maximum

depths at some of these upland creeks exceed 1 m from the combined river flow and precipitation (Fig. 20).

The effect of direct precipitation on the main stem of the Bay is also noticeable. The stations in the lower Bay, where the channel is wide and deep, show negligible differences with or without precipitation (e.g., at Lewes, Fig. 21a). However, at some stations in the upper Bay, where the channel is narrow and shallow, the differences in the surface elevation are noticeable (~25 cm) for a short period (~0.5 day) around the peak surge (Fig. 21b). This station is located at the receiving end of not only water from Delaware River but also some smaller creeks where flash floods have occurred under the heavy precipitation, as shown in Fig. 22. Therefore, our results confirm that the contribution from direct precipitation needs to be incorporated in the compounding flooding events to properly account for the mass budget in rivers and creeks (Santiago-Collazo et al. 2019).

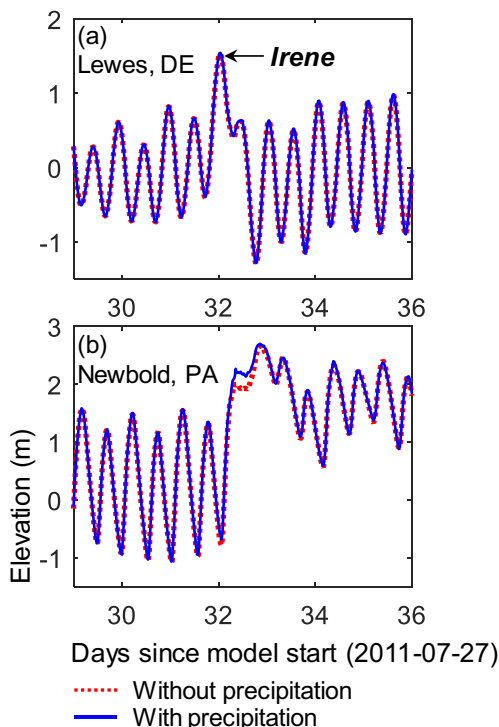


**Fig. 21** Total water levels from baseline and the sensitivity test with precipitation, compared at NOAA stations **a** Lewes, DE (near the Bay mouth) and **b** Newbold, PA (near the Bay head)

#### 4.4 Backwater effect

In Section 4.2, we have examined the river influence on the Bay, and in this section, we will examine the Bay’s influence on rivers and creeks. Backwater effect occurs when the outflowing river water is partially blocked by either the incoming surge from the coast or from nearby rivers. It has important implication on model coupling: if the backwater effect propagates to the boundary between the hydrodynamic and hydrological models, a two-way coupling is then

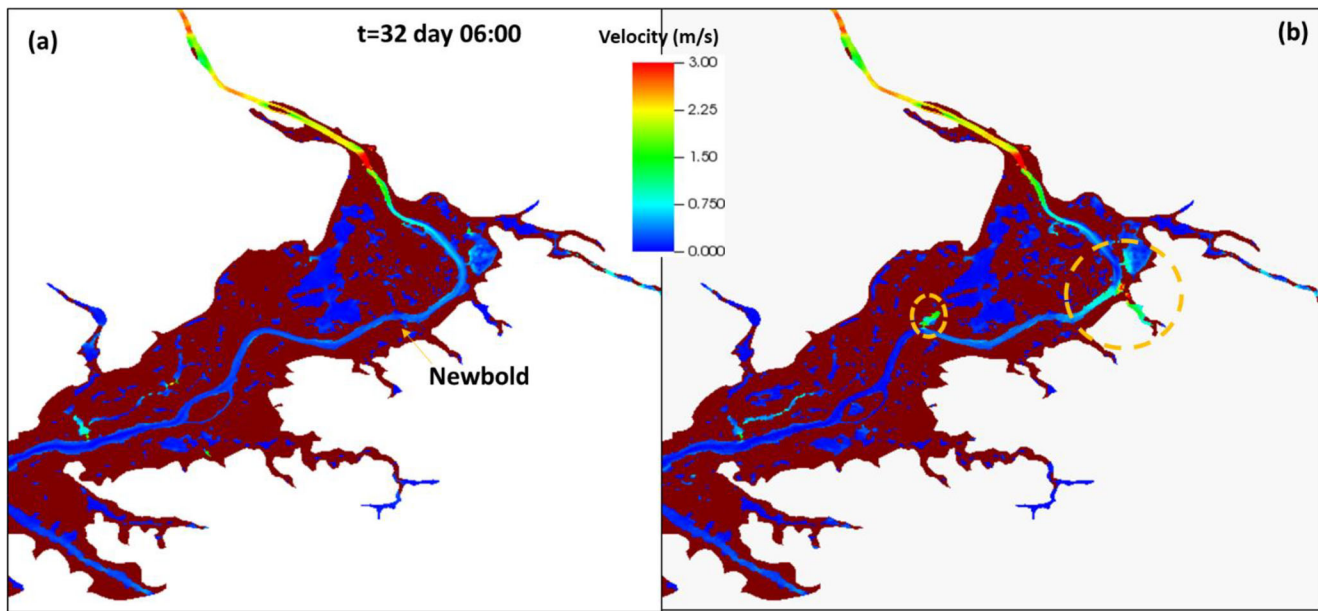


**Fig. 22** Comparison of depth-averaged velocity calculated from **a** baseline; **b** with precipitation. Flash flood that is responsible for the elevation difference at Newbold can be seen in the two circled areas

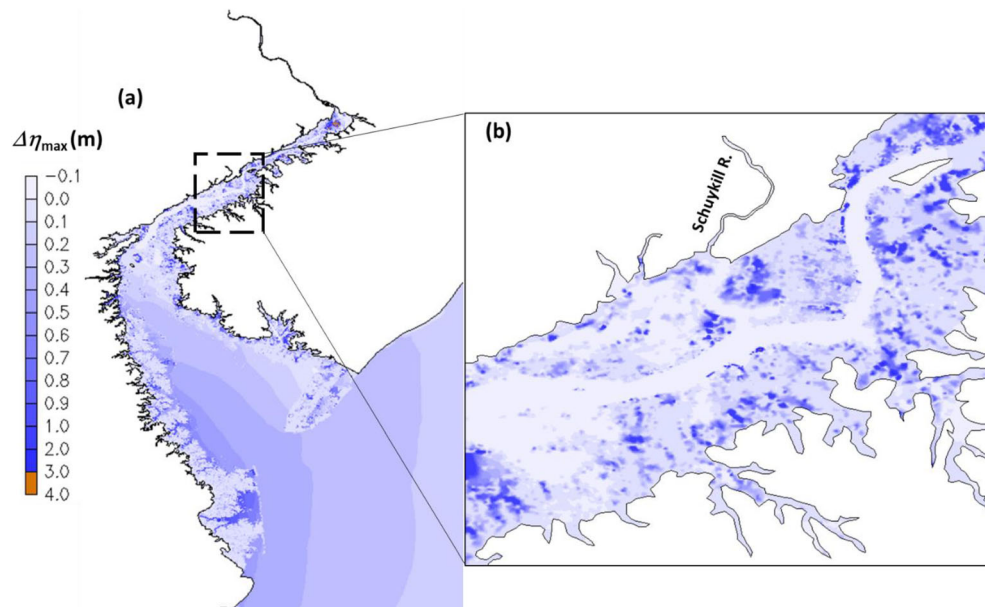
necessary. At the moment, NWM does not receive such information from the hydrodynamic model.

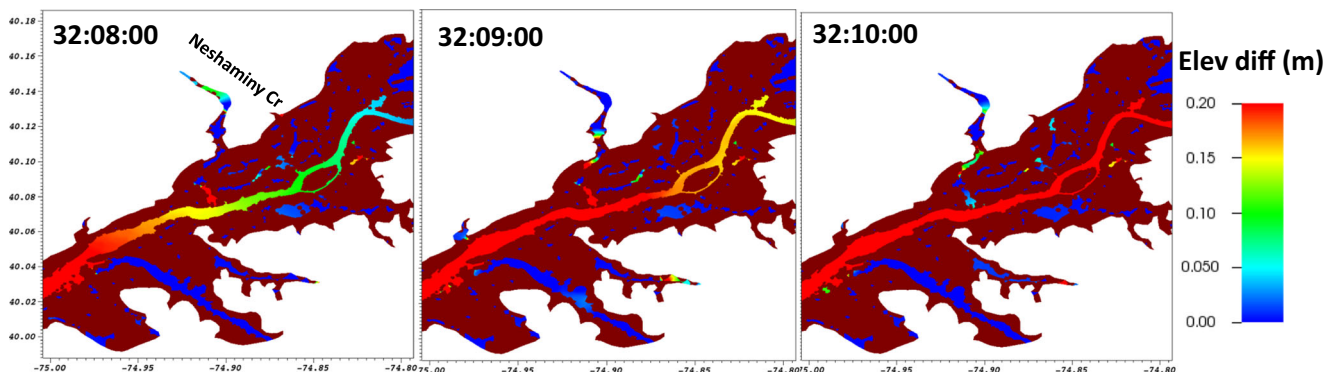
To test the effects of storm surge on the rivers, we conducted a simulation run with reduced wind speed; the maximum  $u$ - and  $v$ -components of the wind are capped at 10 m/s. By comparing the results from this sensitivity run and baseline, we can examine how far the surge effect propagates into rivers and creeks.

Figure 23 shows the maximum of the differences in the predicted elevations between the two runs. Since the wind is

the same inside the Bay, the differences come from the ocean alone. Not surprisingly, the baseline produces higher surges in the lower Bay. However, a non-trivial result is that some differences also occur in large portions of the watershed (Fig. 23a, b). More importantly, non-zero differences have reached the boundary at several locations (e.g., Figure 23b). The elevation differences are generally small in the watershed, about a few centimeters in most places for this event, although 10 s of centimeters or larger differences are also observed in isolated areas (Fig. 23b); the latter are manifestations of “hot

**Fig. 23** Maximum of the differences of elevations (calculated as the differences between the total water depths) for **a** the whole Bay and **b** a zoom in an upper Bay watershed





**Fig. 24** Snapshots of differences of elevation (baseline—reduced), suggesting a sequence of propagation of backwater effect into upstream Neshaminy Creek

spots” of backwater effect. The sequence shown in Fig. 24 suggests that the differences propagate into upstream creeks in the form of multiple wave trains, by taking advantage of the existing waterways (Figs. 23 and 24).

Although generally small in the current study case, the backwater effect may be more significant for larger events. Therefore, a two-way coupling between SCHISM and NWM is necessary in the future. An alternative approach is to extend the SCHISM domain beyond the  $-10\text{ m}$  isobath; however, this approach may be impractical, especially for flat plain areas where the backwater effect can propagate far inland, as in the cases of Hurricanes Harvey (2018) and Florence (2018).

## 5 Conclusions

We have applied a hydrodynamic model to the study of compound flooding events in Delaware Bay during Hurricane Irene (2011). We first demonstrated, using idealized benchmark tests and the field observation, that the model exhibited reasonable skills in simulating fluvial and pluvial processes as well as compound flooding events. We then demonstrated through sensitivity tests the need for tightly coupling riverine processes and precipitation effects in order to properly simulate compound flooding events. The influence of the coastal surge was shown to often propagate far into upstream rivers and creeks, with the backwater effect sometimes reaching the model boundary. Consequently, future work should consider a two-way coupling between the hydrodynamic and hydrological models.

**Acknowledgments** Simulations presented in this paper were conducted using the following computational facilities: (1) SciClone at the College of William and Mary which were provided with assistance from the National Science Foundation, the Virginia Port Authority, Virginia’s Commonwealth Technology Research Fund, and the Office of Naval Research; (2) the Extreme Science and Engineering Discovery Environment (XSEDE; Grant TG-OCE130032), which is supported by National Science Foundation grant number OCI-1053575; (3) the NASA

High-End Computing (HEC) Program through the NASA Advanced Supercomputing (NAS) Division at Ames Research Center; and (4) US Department of Energy’s Scientific Computing Center.

**Funding information** This study was funded by NOAA under Water Initiative (Grant Number NA16NWS4620043).

## References

- Amante C, Eakins BW (2009) ETOPO1 arc-minute global relief model: procedures, data sources and analysis
- Ateljevich E (2014) SELFE Development Status. Methodology for Flow and Salinity Estimates in the Sacramento-San Joaquin Delta and Suisun Marsh, 35th Annual Progress Report. Chapter 2. State of California, Department of Water Resources
- Bilskie MV, Hagen SC (2018) Defining flood zone transitions in low-gradient coastal regions. *Geophys Res Lett* 45:2761–2770. <https://doi.org/10.1002/2018GL077524>
- Carrere L, Lyard F, Cancet M, Guillot A, Picot N (2016) FES 2014, a new tidal model—validation results and perspectives for improvements. In Proceedings of the ESA living planet symposium, pp 9–13
- Chen C, Beardsley RC, Luettich RA, Westerink JJ, Wang H, Perrie W, Xu Q, Donahue AS, Qi J, Lin H, Zhao L (2013) Extratropical storm inundation testbed: intermodel comparisons in Scituate, Massachusetts. *J Geophys Res Oceans* 118(10):5054–5073
- Cho KH, Wang HV, Shen J, Valle-Levinson A, Teng YC (2012) A modeling study on the response of Chesapeake Bay to hurricane events of Floyd and Isabel. *Ocean Model* 49:22–46
- Danielson JJ, Poppenga SK, Tyler DJ, Palaseanu-Lovejoy M, Gesch DB (2018) Coastal National Elevation Database (No. 2018-3037). US Geological Survey
- Danilov S (2012) Two finite-volume unstructured mesh models for large-scale ocean modeling. *Ocean Model* 47:14–25
- Dettinger M (2011) Climate change, atmospheric Rivers, and floods in California – a multimodel analysis of storm frequency and magnitude changes. *J Am Water Resour Assoc* 47(3):514–523. <https://doi.org/10.1111/j.1752-1688.2011.00546.x>
- Dresback KM, Fleming JG, Blanton BO, Kaiser C, Gourley JJ, Tromble EM, Luettich RA, Kolar RL, Hong Y, Van Cooten S, Vergara HJ, Flamig ZL, Lande HM, Kelleher KE, Nemunaits-Monroe KL (2013) Skill assessment of a real-time forecast system utilizing a coupled hydrologic and coastal hydrodynamic model during Hurricane Irene (2011). *Cont Shelf Res* 71:78–94. <https://doi.org/10.1016/j.csr.2013.10.007>

- Groisman PY, Knight RW, Karl TR (2001) Heavy precipitation and high streamflow in the contiguous United States: trends in the twentieth century. *Bull Am Meteorol Soc* 82:219–246
- Groisman PY, Knight RW, Karl TR, Easterling DR, Sun BM, Lawrimore JH (2004) Contemporary changes of the hydrological cycle over the contiguous United States: trends derived from in situ observations. *J Hydrometeorol* 5:64–85
- Jay DA (1991) Green's law revisited: tidal long-wave propagation in channels with strong topography. *J Geophys Res* 96:20585. <https://doi.org/10.1029/91JC01633>
- Jay DA, Flincham EP (1999) A comparison of methods for analysis of tidal records containing multi-scale non-tidal background energy. *Cont Shelf Res* 19(13):1695–1732. [https://doi.org/10.1016/S0278-4343\(99\)00036-9](https://doi.org/10.1016/S0278-4343(99)00036-9)
- Kerr PC, Donahue AS, Westerink JJ, Luettich RA Jr, Zheng LY, Weisberg RH, Huang Y, Wang HV, Teng Y, Forrest DR, Roland A (2013) US IOOS coastal and ocean modeling testbed: inter-model evaluation of tides, waves, and hurricane surge in the Gulf of Mexico. *J Geophys Res Oceans* 118(10):5129–5172
- Kukulka T, Jay DA (2003a) Impacts of Columbia River discharge on salmonid habitat: 1. A nonstationary fluvial tide model. *J Geophys Res* 108
- Kukulka, T., Jay, D.A., 2003b. Impacts of Columbia River discharge on salmonid habitat: 2. Changes in shallow-water habitat *J Geophys Res* 108
- Lanzoni S, Seminara G (1998) On tide propagation in convergent estuaries. *J Geophys Res Oceans* 103:30793–30812. <https://doi.org/10.1029/1998JC00015>
- Le Roux DY, Sene A, Rostand V, Hanert E (2005) On some spurious mode issues in shallow-water models using a linear algebra approach. *Ocean Model* 10(1–2):83–94
- Liu Z, Zhang Y, Wang HV, Wang Z, Ye F, Huang H, Sisson M (2018) Impact of small-scale structures on estuarine circulation. *Ocean Dyn* 68(4):509–533. <https://doi.org/10.1007/s10236-018-1148-6>
- Lynett PJ, Gately K, Wilson R, Montoya L, Adams L, Arcas D, Aytore B, Bai Y, Bricker JD, Castro MJ, Cheung K, David C, Dogan G, Escalante C, Gonzalez FI, Gonzalez-Vida J, Grilli ST, Heitmann TW, Horrillo J, Kanoğlu U, Kian R, Kirby JT, Li W, Macaas J, Nicolsky DJ, Ortega S, Pampell-Manis A, Park Y, Roeber V, Sharqivand N, Shelby M, Shi F, Tehranir B, Tolkova E, Thio H, Velioglu D, Yalciner A, Yamazaki Y, Zaytsev A, Zhang Y (2017) Inter-model analysis of tsunami-induced coastal currents. *Ocean Model* 114:14–32. <https://doi.org/10.1016/j.ocemod.2017.04.003>
- Magnusson L, Bidlot JR, Lang ST, Thorpe A, Wedi N, Yamaguchi M (2014) Evaluation of medium-range forecasts for Hurricane Sandy. *Mon Weather Rev* 142(5):1962–1981
- McKeon BJ, Swanson CJ, Zagarola MJ, Donnelly RJ, Smits AJ (2004) Friction factors for smooth pipe flow. *J Fluid Mech* 511:41–44
- Moftakhar HR, Jay DA, Talke SA, Kukulka T, Bromirski PD (2013) A novel approach to flow estimation in tidal rivers. *Water Resour Res* 49:4817–4832. <https://doi.org/10.1002/wrcr.20363>
- Moftakhar HR, AghaKouchak A, Sanders BF, Allaire M, Matthew RA (2018) What is nuisance flooding? Defining and monitoring an emerging challenge. *Water Resour Res.* <https://doi.org/10.1029/2018WR022828>
- Moftakhar H, Schubert JE, AghaKouchak A, Matthew R, Sanders BF (2019) Linking statistical and hydrodynamic modeling for compound flood Hazard assessment in tidal channels and estuaries. *Adv Water Resour.* <https://doi.org/10.1016/j.advwatres.2019.04.009>
- NTHMP (2012) Proceedings and results of the 2011 NTHMP (National Tsunami Hazard Mitigation Program) model benchmarking workshop. Boulder: US Depart. of Commerce/NOAA/NTHMP, NOAA Special Report 436p
- Santiago-Collazo FL, Bilskie MV, Hagen SC (2019) A comprehensive review of compound inundation models in low-gradient coastal watersheds. *Environ Model Softw* 119:166–181. <https://doi.org/10.1016/j.envsoft.2019.06.002>
- Shapiro R (1970) Smoothing, filtering, and boundary effects. *Rev Geophys* 8(2):359–387
- Sobel AH, Camargo SJ, Hall TM, Lee C-Y, Tippett MK, Wing AA (2016) Human influence on tropical cyclone intensity. *Science* 353:242–246. <https://doi.org/10.1126/science.aaf6574>
- Stelling GS, Duinmeijer SPA (2003) A staggered conservative scheme for every Froude number in rapidly varied shallow water flows. *Int J Numer Meth Fluids* 43:1329–1354. <https://doi.org/10.1002/fld.537>
- Teng J, Jakeman AJ, Vaze J, Croke BF, Dutta D, Kim S (2017) Flood inundation modelling: a review of methods, recent advances and uncertainty analysis. *Environ Model Softw* 90:201–216
- Trenberth KE (2011) Changes in precipitation with climate change. *Clim Res* 47:123–138. <https://doi.org/10.3354/cr00953>
- Trenberth KE, Cheng L, Jacobs P, Zhang Y, Fasullo J (2018) Hurricane Harvey links to ocean heat content and climate change adaptation. *Earths Futur.* <https://doi.org/10.1029/2018EF000825>
- Umlauf L, Burchard H (2003) A generic length-scale equation for geophysical turbulence models. *J Mar Res* 61(2):235–265
- Wing OJ, Sampson CC, Bates PD, Quinn N, Smith AM, Neal JC (2019) A flood inundation forecast of Hurricane Harvey using a continental-scale 2D hydrodynamic model. *J Hydrol X* 4:100039. <https://doi.org/10.1016/j.hydra.2019.100039>
- Ye F, Zhang YJ, Wang HV, Friedrichs MA, Irby ID, Alteljevich E, Valle-Levinson A, Wang Z, Huang H, Shen J, Du J (2018) A 3D unstructured-grid model for Chesapeake Bay: importance of bathymetry. *Ocean Model* 127:16–39
- Ye F, Zhang Y, He R, Wang ZG, Wang HV, Du J (2019) Third-order WENO transport scheme for simulating the baroclinic eddying ocean on an unstructured grid. *Ocean Model* 143:101466. <https://doi.org/10.1016/j.ocemod.2019.101466>
- Ye F, Zhang Y, Yu H, Sun W, Moghimi S, Myers EP, Nunez K, Zhang R, Wang HV, Roland A, Martins K, Bertin X, Du J, Liu Z (2020) Simulating storm surge and compound flooding events with a creek-to-ocean model: importance of baroclinic effects. *Ocean Model* 145. <https://doi.org/10.1016/j.ocemod.2019.101526>
- Yu H-C, Zhang Y, Yu JCS, Teng C, Sun W, Ye F, Wang HV, Wang Z, Huang H (2017) Simulating multi-scale oceanic processes around Taiwan on unstructured grids. *Ocean Model* 112:72–93. <https://doi.org/10.1016/j.ocemod.2017.09.007>
- Zeng X, Zhao M, Dickinson RE (1998) Intercomparison of bulk aerodynamic algorithms for the computation of sea surface fluxes using TOGA COARE and TAO data. *J Clim* 11(10):2628–2644
- Zhang Y, Baptista AM (2008a) SELFE: A semi-implicit Eulerian-Lagrangian finite-element model for cross-scale ocean circulation. *Ocean Model* 21(3–4):71–96
- Zhang Y, Baptista AM (2008b) An efficient and robust tsunami model on unstructured grids. Part I: inundation benchmarks. *Pure Appl Geophys* 165:1–20
- Zhang Y, Witter RW, Priest GP (2011) Tsunami-tide interaction in 1964 Prince William Sound Tsunami. *Ocean Model* 40:246–259
- Zhang Y, Ateljevich E, Yu HC, Wu CH, Jason CS (2015) A new vertical coordinate system for a 3D unstructured-grid model. *Ocean Model* 85:16–31
- Zhang Y, Ye F, Stanev EV, Grashorn S (2016) Seamless cross-scale modeling with SCHISM. *Ocean Model* 102:64–81